Flow Kinematics in Variable-Height Rotating Cylinder Arrays

Anna E. Craig
Department of Mechanical Engineering,
Stanford University,
Stanford, CA 94035
e-mail: craig0a@stanford.edu

John O. Dabiri
Professor
Department of Civil and
Environmental Engineering;
Department of Mechanical Engineering,
Stanford University,
Stanford, CA 94035

Jeffrey R. Koseff
Professor
Department of Civil and
Environmental Engineering,
Stanford University,
Stanford, CA 94035

Experimental data are presented for large arrays of rotating, variable-height cylinders in order to study the dependence of the three-dimensional mean flows on the height heterogeneity of the array. Elements in the examined arrays were spatially arranged in the same staggered paired configuration, and the heights of each element pair varied up to ±37.5% from the mean height (kept constant across all arrays), such that the arrays were vertically structured. Four vertical structuring configurations were examined at a nominal Reynolds number (based on freestream velocity and cylinder diameter) of 600 and nominal tip-speed ratios of 0, 2, and 4. It was found that the vertical structuring of the array could significantly alter the mean flow patterns. Most notably, a net vertical flow into the array from above was observed, which was augmented by the arrays' vertical structuring, showing a 75% increase from the lowest to highest vertical flows (as evaluated at the maximum element height, at a single rotation rate). This vertical flow into the arrays is of particular interest as it represents an additional mechanism by which high streamwise momentum can be transported from above the array down into the array. An evaluation of the streamwise momentum resource within the array indicates up to a 56% increase in the incoming streamwise velocity to the elements (from the lowest to highest ranking arrays, at a single rotation rate). These arrays of rotating cylinders may provide insight into the flow kinematics of arrays of vertical axis wind turbines (VAWTs). In a physical VAWT array, an increase in incoming streamwise flow velocity to a turbine corresponds to a (cubic) increase in the power output of the turbine. Thus, these results suggest a promising approach to increasing the power output of a VAWT array.
[DOI: 10.1115/1.4033676]

1 Introduction

In recent years, it has been shown that for specific regimes of geometric spacing, rotational orientation, Reynolds number, and rotation rate, paired rotating cylinders can suppress bluff-body vortex shedding and can exhibit increased lift coefficients and decreased drag coefficients (see Refs. [1–6], among others). Motivated by the potential implications that such positive interactions between rotating elements could have for VAWT arrays (see Refs. [7–9], among others), recent work was completed on large arrays of finite-height rotating cylinders [10]. In that study, the cylinders were of uniform height, and the spatial and rotational configurations of the elements were varied. It was found that the rotation of the cylinders drove the formation of streamwise and transverse flow patterns between cylinders, and that net time–space averaged transverse and vertical flows existed within the developed flow regions of the arrays.

The present study is a direct extension of this prior work: large arrays of rotating cylinders are again considered, but the spatial and rotational configurations are held constant while vertical structuring of the arrays is achieved by varying the height of the elements within the arrays.

Significant prior work on heterogeneous-height arrays has been completed, particularly in the context of aquatic natural canopies (e.g., Ref. [11]) and terrestrial urban canopies (e.g., Refs. [12–17]). Most notably, Xie et al. [14] examined arrays of spatially staggered rectangular blocks of either homogeneous heights or heterogeneous heights, randomly chosen from a normal distribution such that the mean height of the heterogeneous array was equal to the height of the homogeneous array (H). It was found that the time–space averaged velocity below H was very similar between the two arrays, but that above H the heterogeneous array showed lower velocities than the homogeneous array. This is not surprising given that within the heterogeneous-height array, tall elements still exerted drag on the flow above H. As a result, however, the time–space averaged velocity profile showed a much weaker inflection in transitioning from within-array to above-array flow, and thus a significantly reduced shear layer. The reduced shear layer also reduced the magnitude of the peak time–space averaged turbulent kinetic energy which was observed to occur at the height of the tallest elements in the array rather than at H.

Jiang et al. [15] examined the spatially square arrays of blocks with varying degrees of height heterogeneity, while maintaining the same mean element height. Largely in keeping with the results reported by Xie et al. [14], it was observed that with increasing height variation of the elements in a square array, the time–space averaged flow velocity was increased below the mean height and decreased above the mean array height.

Finally, Hagishima et al. [16] examined the spatially staggered and square arrays with either homogeneous-height elements or elements of two different heights, again maintaining the same mean element height in all cases. It was shown that while the displacement height, roughness length, and coefficient of drag of the arrays varied most strongly between homogeneous-height and heterogeneous-height arrays, there was also notable variation between heterogeneous arrays of different vertical structures (i.e., the tall elements in a square pattern versus the tall elements in a staggered pattern).

Taking these studies into consideration, the present study focuses on arrays composed of elements of three distinct heights to create four different vertically structured arrays, maintaining the same mean array height between arrays. Focus will be placed on the time–space averaged characteristics of the flow in the array, specifically in relation to the momentum resource available within the array.

The focus on time–space averaged flow characteristics and particularly the momentum resource is motivated by the potential implications of the study for VAWT arrays. While it was concluded in Ref. [10] that direct analogies between the examined rotating cylinder arrays and VAWT arrays should not be drawn, the experimental model simplifications are comparable to some of the numerical model simplifications under consideration for large-

Contributed by the Fluids Engineering Division of ASME for publication in the Journal of Fluids Engineering. Manuscript received January 28, 2016; final manuscript received May 12, 2016; published online July 15, 2016. Assoc. Editor: Mark F. Tachie.

eddy simulations (LESs) focused on large, three-dimensional (3D) arrays (e.g., Refs. [18–20]). In particular, Shamsoddin and Porte-Agel [19] compare an actuator line model, in which each blade is represented by a moving line of point forces, and an actuator swept-surface model, in which the time-averaged forcing of the blades is distributed over the cylindrical surface swept out by the blades. It was shown that the actuator line model was better able to capture the unsteady-periodic nature of the wake, and in particular showed faster wake recovery as a result of better modeling of the wake turbulence intensity. However, the actuator swept-surface model captured mean flow characteristics reasonably well and was the lower-computational cost model. In an LES of a mixed turbine wind farm, Archer et al. [20] employed the actuator swept-surface model for the (20) shorter, under-story VAWTs and an actuator line model for the (single) taller, upper-story horizontal axis wind turbines, highlighting the accuracy/computing cost balance which currently still faces LES studies.

As the distribution of the turbine forcing across a cylindrical surface in numerical simulations is strongly analogous to the experimental model of the turbines as cylinders, the prior [10] and present work may be considered similar to such LES studies of a large-scale VAWT array, in which the near-"turbine" details are not captured, but the net effect on the flow may be considered qualitatively informative, as a low-order approximation.

The remainder of the paper is organized as follows: Section 2 gives a brief outline of the experimental methods, including notation, experimental setup, and uncertainty quantification. Section 3 presents the results of the experiments, beginning with a quantification of the array performances (Sec. 3.1), followed by closer examinations of the mean vertical flow patterns in the arrays (Sec. 3.2) and the turbulence characteristics in the arrays (Sec. 3.3). Section 4 summarizes the key results and discusses potential avenues of further research.

2 Experimental Methods

The present work is a direct extension of the work previously described and reported in Ref. [10], and therefore, only a brief description of the experimental setup and methodology will be given here. Also, the supplementary material in Ref. [10] provides a detailed discussion of the relationship of the present experimental model to a physical VAWT array, in particular discussing the following: Reynolds number effects, flow-driven versus externally supplied element rotation, the constant rotation rate of elements through the array, and the geometry of the elements.

2.1 Notation. The nondimensional rotation rate is defined to be $\alpha = D\Omega/2u_0$, where D is the cylinder diameter, Ω is the rotational speed of the cylinder, and u_0 is the freestream velocity. The pertinent Reynolds number is defined by the cylinder diameter and freestream velocity, that is, $\mathrm{Re} = u_0 D/\nu$, where ν is the kinematic viscosity of the working fluid.

The sequential time–space decomposition of a variable is written as $\theta = \langle\bar{\theta}\rangle + \tilde{\bar{\theta}} + \theta'$, where the overline denotes a time average, the prime denotes a deviation from the time average, the brackets denote a spatial average, and the tilde denotes a deviation from the spatial average (adopting the notation in Ref. [21]).

2.2 Experimental Setup. The coordinate system used in this work takes the positive x direction to be aligned with the freestream flow and the z direction to be vertically upward, leaving the y direction aligned transversely. The origin of the coordinate system is placed at the transverse center of the first row in the array, at the bottom of the elements.

The arrays examined consisted of 532 circular cylindrical elements (266 element pairs) arranged in 59 rows. The elements were 1.27 cm in diameter (D). Unless otherwise indicated, all lengths in this work are normalized by the element diameter. Staggering of the pairs between rows yielded five pairs per row or four pairs per row (alternating by row, Fig. 1). Of these, the central three or two pairs, respectively, in each row were externally rotated, with the remaining pairs at the sides of each row left stationary in order to act as "buffer" regions. The rotation of the elements was such that the inner edges of the cylinders in a pair moved in the downstream direction (referred to as the "reverse doublet" configuration in prior literature [1,10]). The spatial configuration (including element spacing) was motivated by the work on paired cylinders by Chan et al. [1] and on VAWT arrays by Kinzel et al. [9] (see Ref. [10] for further details). The choice of the reverse doublet rotational configuration was based on the results of Craig et al. [10], which indicated this configuration to have the best interaction characteristics with the flow above the arrays.

Element rotation was accomplished by creating chains of spur gears, sandwiched in place between a bottom and top plate, as shown in Fig. 2(*a*). Some of the spur gears were fitted with shafts that protruded through the top plate and provided a mounting point for the elements above the top plate. At the ends of the gear chains, the spur gears were fitted with very long shafts which also protruded through the top plate and were connected to direct current motors above the array. Controlling the voltage supplied to the motors allowed the rotation rate of the gear chain and therefore the elements to be controlled. Data were collected with the elements driven to rotation rates of $\alpha = [0, 2, 4]$.

The entire setup was placed into the recirculating water flume of the Bob and Norma Street Environmental Fluid Mechanics Laboratory at Stanford University, as shown in Fig. 2(*b*). As the spur gear sandwich had a finite thickness, additional raised plates were used to fill the flume in front, in back, and to the sides of the setup so that a consistent offset bottom was formed. The most upstream plate was angled so as to provide a ramp up to the offset bottom and also provide a trip for the boundary layer. See Supplemental Materials tab for this paper on the ASME Digital Collection.

Three element heights were used to create the vertical structures of the arrays: a short element 5D in height, an average element 8D in height, and a tall element 11D in height. The arrays were created such that the average element height over the array was 8D. Four vertical structures were considered: "uniform," in which all elements were of average height, "sawtooth," in which height was varied by row: short, average, tall, short, average, tall, etc., "wedge," in which short elements and tall elements were used to create nested "V" shapes, with the openings in the upstream position, and "random," in which a random number generator was used to randomly assign each position to contain a small, average, or tall element pair. These vertical array structures are illustrated in Fig. 1. The homogeneous and random vertical structures were chosen so as to be consistent with the previous studies. The sawtooth vertical structure was chosen for its simplicity, ideally allowing relatively easy interpretation of the results. The wedge vertical structure was motivated by the work presented in Ref. [22], which suggests that the V shape may result in beneficial channeling between rotating elements.

Two-dimensional particle image velocimetry was used to collect data in both vertical (x–z) planes and horizontal (x–y) planes. The data were taken at a streamwise position far downstream of the leading edge of the array. The horizontal data were collected at the same three heights in all heterogeneous-height arrays: 4D, 7D, and 10D from the offset bottom/base of the elements. In the homogeneous-height array, six horizontal sheets of data were collected at 2.0D, 6.0D, 4.0D, 7.5D, 8.5D, and 10.0D from the offset bottom. The vertical sheet data were not collected at the same transverse locations between arrays, given the requirements of reasonably capturing the variation associated with the different vertical structures; however, the distribution of the data sheets relative to the elements (i.e., the number of data sheets taken through the centers of elements versus between elements in a pair versus between pairs of elements) was matched when taking spatial averages so as to be easily comparable across arrays. The transverse locations captured are indicated in Fig. 1 for each of the array

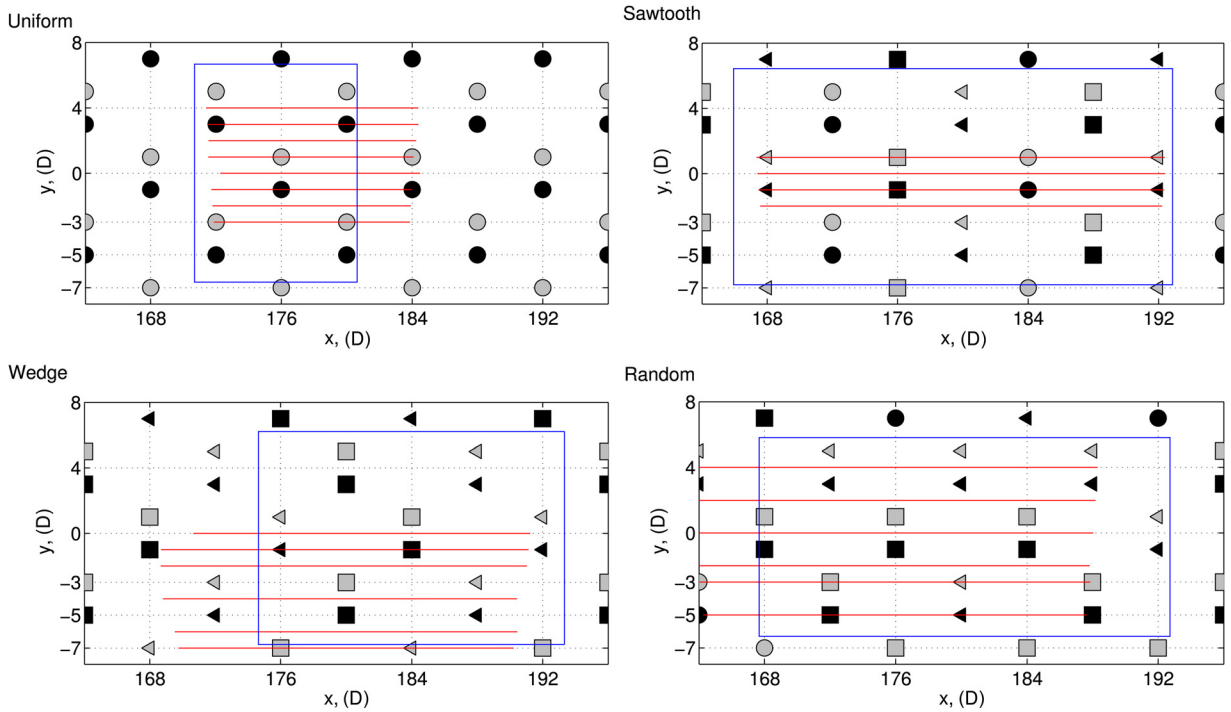

Fig. 1 Schematics of the spatial, rotational, and height configurations of the arrays (within the region of interest). Each symbol indicates the position of an element. The color of the symbol indicates the rotational direction as viewed from above: black is clockwise and gray is counterclockwise. The symbol indicates the height of the element: ◁ indicates a short element, ○ indicates an average element, and □ indicates a tall element. The red (light gray) lines indicate the transverse locations and streamwise extents of the vertical data sheets taken in each array. The blue (dark gray) box indicates the position and extent of the horizontal data sheets taken.

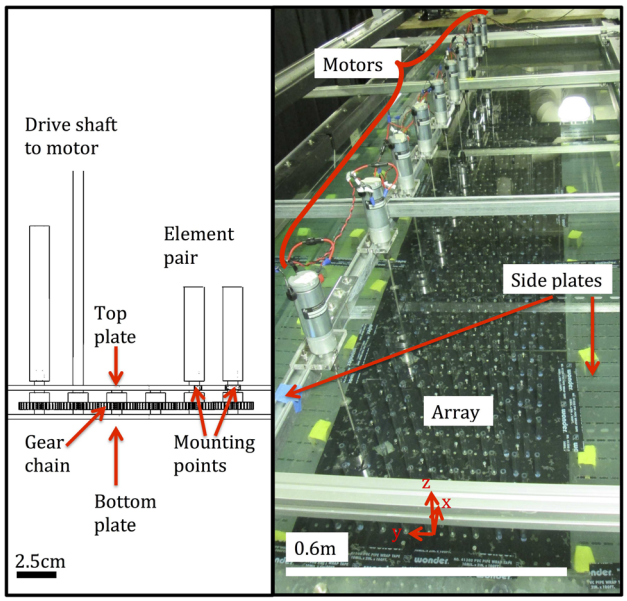

Fig. 2 Experimental setup illustrations. Left: close-up sketch showing element mounting to gears and plate structure holding gears in place. Right: photo of full array in the flume. Figure adapted from Ref. [10].

configurations. At each measurement location, 512 image pairs were captured at a rate of 0.5 Hz.

All velocities are normalized by the freestream velocity, u_0 (0.0468 m/s for the heterogeneous-height arrays and 0.0447 m/s for the uniform height array, the difference arising from the fact that the data were collected in two separate installations of the setup in the flume, with minor variations between installations). The resulting Reynolds numbers were, therefore, 594 and 568, respectively. Examination of the temporal and spatial power spectral densities indicated that the flow within the arrays was fully turbulent at these Reynolds numbers. See Supplemental Materials tab for this paper on the ASME Digital Collection.

2.3 Measurement Uncertainty. A circular, moving block bootstrap (see Refs. [23–25]) was used to provide uncertainty estimates for the majority of the statistics examined in the present work. The one exception is the "performance" statistic for the arrays. The metric chosen involves selecting only certain data points with respect to the positions of the elements; therefore, the bootstrapping method was adapted to also take into consideration the uncertainties associated with correct alignment of the collected data within the array (and therefore with respect to the element positions).

This quantification of measurement uncertainty was based on a thorough analysis including the propagation of all explicitly quantifiable uncertainties (e.g., camera calibration) and the comparative estimation of uncertainties not explicitly quantifiable (e.g., day-to-day variations) [10]. From this analysis, it was found that the statistical variations were the dominant source of explicitly quantifiable uncertainties (in all but the performance metric case, where the additional global alignment uncertainty was significant and has therefore been retained). Furthermore, it was found that the estimated experimental variation uncertainties were typically of the same order of magnitude as the statistical uncertainties. For the present set of measurements, however, the full complement of data necessary to determine an estimate for the experimental variations was not available. The presented uncertainties should, therefore, be treated as a somewhat optimistic estimate as they do not include any experimental variations or bias correction.

3 Results

3.1 Quantifying Array Performance. In order to quantitatively compare the flow in the different arrays, a performance metric was defined which was motivated by the potential implications of the present work for the VAWT arrays. For wind turbine arrays, the streamwise velocity spatially averaged over the frontal area of the turbine may be taken as an indicator of the power resource available within the array [26,27]. In the present work, the following metric is proposed for quantitatively comparing the arrays:

$$C_{u_{\text{in}}} = \frac{\sum_{\text{elements}} \int_0^h \langle \bar{u} \rangle|_{\text{in}} dz}{\sum_{\text{elements}} h} \tag{1}$$

Conceptually, this metric quantifies the mean incoming streamwise flow per unit frontal area of the elements. More explicitly, the mean incoming streamwise flow, $\langle \bar{u} \rangle|_{\text{in}}$, was computed from the horizontal sheet data as a partial-spatial average of $\bar{u}$ taken $1.25D$ upstream of the elements over the projected $1D$ transverse span of an element. This value was computed for each element contained within the horizontal data sheets, at each of the horizontal data sheet heights (whatever the height of the element in question). A spline fit of the metric was then taken through the measurements, including a zero flow velocity at the bottom of the array. The splined metric was then integrated over the height of the element in question, and the height of the element (h) was also recorded. The total integrated performance over all measured elements was then divided by the total height over which the metric had been integrated (and the $1D$ width of the elements) in order to yield an average $\langle \bar{u} \rangle|_{\text{in}}$ per unit frontal area (defined in Eq. (1) as $C_{u_{\text{in}}}$ for notational convenience). The results of this analysis are given in Fig. 3, where the metric has been normalized by the maximum performance (across all arrays and rotation rates) for ease of comparison.

There are a number of interesting comparisons which may be drawn from this analysis. The most immediately obvious comparison is the substantially improved performance observed in the wedge array as compared to the other vertical structures, for both $\alpha = 2$ and $\alpha = 4$. Comparing the $\alpha = 2$ performances, the next best-performing uniform array drops 20% in performance, while the worst-performing sawtooth array drops 36% in performance. This highlights an important observation: the improvement in performance in an array containing tall elements is not merely a result of accessing higher velocity resources further from the bottom of the array. In comparison to the uniform height array, the introduction of tall elements and vertical structuring can either improve or deteriorate the array performance.

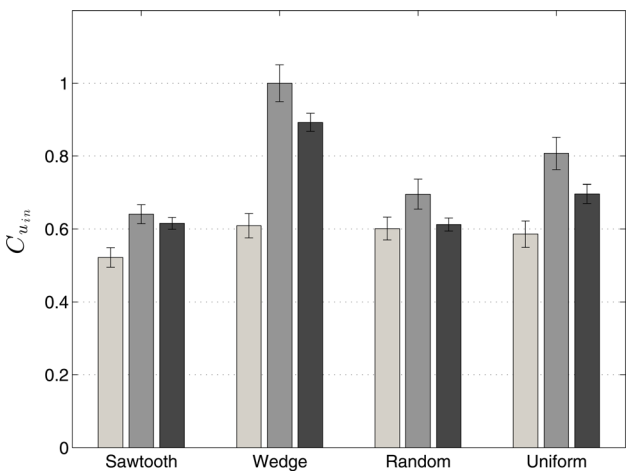

Fig. 3 Comparison of $C_{u_{\text{in}}}$ (normalized to maximum measured value) across arrays and rotation rates. Light gray indicates $\alpha = 0$, medium gray indicates $\alpha = 2$, and dark gray indicates $\alpha = 4$.

Another interesting observation is that all arrays perform best at $\alpha = 2$, with the performance at $\alpha = 4$ being significantly lower, even dropping so low in the random array as to be at the same level as the $\alpha = 0$ case. Examining the mean velocity fields $\bar{u}$ and $\bar{v}$ in the horizontal planes of data, the reason for the drop in performance is readily apparent. The flow immediately surrounding each cylinder is entrained such that it matches the direction of the cylinder (i.e., upstream moving flow near the upstream moving edge of the cylinder, negative transversely moving flow near the negative transversely moving edge of the cylinder, etc.) In the case of $\alpha = 2$, the upstream/reduced streamwise flow near the upstream moving edges of the cylinders is relatively small and confined to just the transverse sides of the cylinders. In the case of $\alpha = 4$, the upstream/reduced streamwise flow regions have expanded and have been swept around by the transverse component of the induced flow to also partially encompass the fronts of the cylinders, where the performance measurement is being made. For this reason, in the remainder of the work, further analysis will focus primarily on the $\alpha = 2$ data.

Based on the previous work on homogeneous-height arrays, there are two flow characteristics within the array which may be considered pertinent in determining the performance of an array: the vertical flux of streamwise momentum from above the array down into the array and the horizontal redistribution or mixing of the influx momentum within the array. These two characteristics will be examined more closely in Secs. 3.1.1 and 3.1.2, respectively.

3.1.1 Vertical Flux of Streamwise Momentum. The (integral) vertical flux of streamwise momentum may be decomposed into three contributions: a mean-driven flux $\langle \bar{u} \rangle \langle \bar{w} \rangle$, a Reynolds stress-driven flux $\langle \overline{u'w'} \rangle$, and a dispersion-driven flux $\langle \tilde{\bar{u}} \tilde{\bar{w}} \rangle$. The profiles of each term are given in Fig. 4. Note that here z is normalized by the height of the tallest element in the array (H_{max}), rather than by the cylinder diameter, in order to permit clearer comparison between the heterogeneous-height and homogeneous-height arrays.

The first notable feature of these profiles is the dominant role played by the mean-driven flux in all arrays. In the case of the wedge array at the top of the highest elements, the mean-driven flux is over four times the magnitude of the Reynolds stress-driven flux. For all arrays, the Reynolds stress-driven flux is the second largest contributor to the vertical flux, with the dispersion-driven flux being relatively negligible.

One very interesting feature in comparing the different arrays is that the mean-driven flux varies significantly between the different arrays, and intriguingly, the magnitudes of mean-driven vertical flows at the top of the arrays appear to follow the same ordering as the performance of the array. More rigorously, taking the linear correlation between the computed performance metric $C_{u_{\text{in}}}$ and the time–space averaged vertical flow evaluated at the maximum height of each array ($\langle \bar{w} \rangle|_{z=H_{\text{max}}}$) for $\alpha = 2$, the correlation coefficient is $R^2 = 0.92$ across the four array configurations. Motivated by this, the patterns of mean vertical flow within the arrays will be examined in some depth in Sec. 3.2, particularly in the context of how the vertical structure of the array influences this vertical flow.

Examining the Reynolds stress-driven fluxes, there is a distinctive peak in the flux at the height of the highest elements in all arrays. Below this peak, the profile in the uniform height array decays relatively monotonically. In contrast, the heterogeneous-height arrays show secondary peaks at lower heights. In the wedge array, there is a clear secondary peak at the height of the short elements. In the sawtooth array, there is a notable secondary peak at the height of the average elements and a very slight but still identifiable peak at the height of the short elements. The random array, interestingly, shows a rather vertically extensive "peak" over the region between the average and short element heights. Motivated

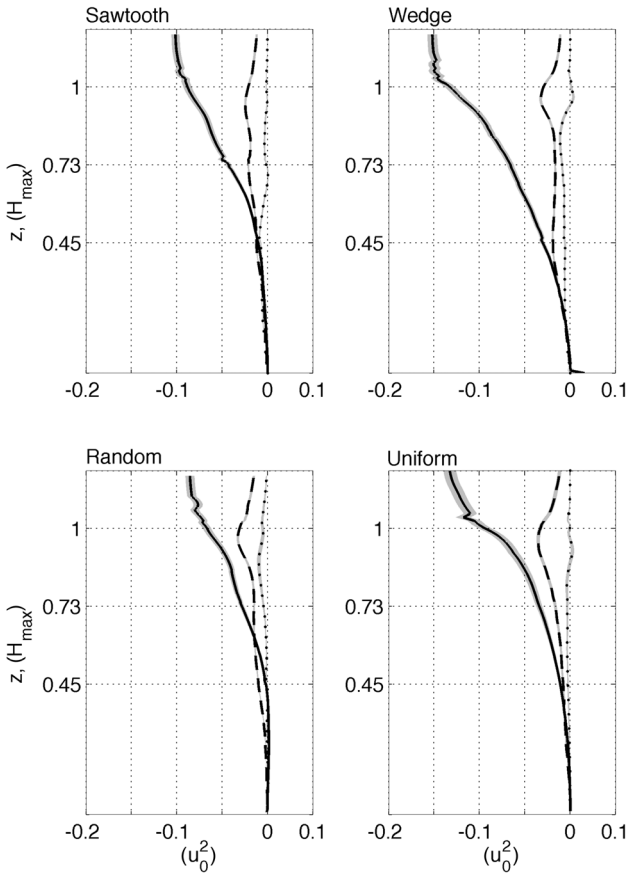

Fig. 4 Comparison of streamwise momentum flux terms for $\alpha = 2$. Solid line: $\langle \bar{u} \rangle \langle \bar{w} \rangle$, dashed line: $\langle u'w' \rangle$, and dotted line: $\langle \tilde{u}\tilde{w} \rangle$. Note that on this scale, for the sawtooth, wedge, and random arrays, the tallest elements are at height 1, the average elements are at height 0.73, and the short elements are at height 0.45, as indicated by the grid lines. While these latter two heights have no meaning for the uniform array, the grid lines have been retained for easier comparison between arrays.

by these features, the turbulence characteristics within the arrays are examined in more detail in Sec. 3.3.

3.1.2 Horizontal Flow Patterns. The other characteristic which has been previously identified as important to the performance of an array is the horizontal pattern of flow within the array which can act to either favorably channel the injected momentum through the array or unfavorably divert the momentum. While the same spatial and rotational configurations of the elements in all arrays considered here lead to the same qualitative patterns in the arrays, there are subtle differences. To illustrate these, Fig. 5 presents the horizontal flows in the best-performing wedge and worst-performing sawtooth arrays, at each of the three measurement heights. See Supplemental Materials tab for this paper on the ASME Digital Collection.

At the highest data sheet ($z = 10D$), for both arrays, it can be qualitatively seen that the transverse flow is much smaller than the streamwise flow, as evidenced by the largely streamwise-aligned streamlines. Certainly, there are transverse flows, mainly converging in front of and diverging behind each pair, but these are largely localized effects. The one difference is for the wedge array where there is some channeling between pairs.

The middle data sheet ($z = 7D$) now intersects the average height elements of the sawtooth array, and the interactions between the pairs of elements can be seen. There does seem to be some level of large-scale pattern to the transverse flows, as there is largely negative transverse flow in the negative y direction from the centerline and positive transverse flow in the positive y direction from the centerline. This, however, is by no means consistent, showing significant "patchiness" of transverse flow direction. The wedge array, on the other hand, shows relatively clear and strong large-scale patterns. No medium height elements exist to disrupt the channeling of flow from one pair of tall elements to the next within the wedge, and then behind the wedge, the transverse divergence of flow across the centerline is uninterrupted. The overall result is very clean channeling of flow from one wedge of elements to the next.

The lowest data sheet ($z = 4D$) shows the clearest differences. At this height in the array, the spatial and rotational patterns of the elements as intersected by the data sheet are exactly the same between the arrays. Any difference between the patterns, therefore, must be attributed to 3D effects. In the sawtooth array, the patchiness of the transverse flow has increased, and as a result, the streamlines through the array have become very "meandering." In contrast, the wedge array still shows much the same transverse flow split behind the wedge of tall elements. This indicates that the transverse flow patterns established at the higher heights in the array are influencing the transverse flow patterns at the lower heights in the array. As a result, the streamlines within the wedge array appear to be significantly more channeled from one pair of cylinders to the next.

In order to quantify these qualitatively observed features, the "meander" of the streamlines (denoted for simplicity m) was computed to be the difference between the path length of a streamline (L_{path}) and the straight line distance between the starting and ending points of the streamline (L_{straight}), normalized by the latter: $m = (L_{\text{path}} - L_{\text{straight}})/L_{\text{straight}}$. Streamlines were initiated at every point in the data field. The median of m was then taken over all streamlines, and this was plotted against the average incoming streamwise velocity for elements intersecting that data sheet ($\langle \bar{u} |_{\text{in}}$, taken across the projected element span $1.25D$ upstream). Figure 6 presents the results of this comparison, in log–log scale, including all array configurations at $\alpha = 2$.

Clearly, as meander of the flow through the array increases, the performance of the array decreases and vice versa. Fitting the log–log data with a linear fit indicates the following correlation, with $R^2 = 0.86$: $\langle \bar{u} |_{\text{in}} = 003(\text{median}(m))^{-0.35}$. At present, a mathematical justification for the -0.35 exponent is not proposed.

3.2 Vertical Flow Patterns. As mentioned in Sec. 3.1.1, a linear correlation coefficient of $R^2 = 0.92$ exists between the computed performance metric $C_{u_{\text{in}}}$ and the time–space averaged vertical flow evaluated at the maximum height of each array ($\langle \bar{w} \rangle |_{z=H_{\max}}$) for $\alpha = 2$. Motivated by this, a simply empirical model is here developed in order to provide a kinematic differentiation between the vertical structuring of the arrays with respect to the observed vertical flows.

Figure 7 presents the time-averaged vertical flow field at the centerline of the arrays and (where available) through the counterclockwise rotating cylinders closest to the centerline. Qualitative examination of the streamlines suggested that the angle of the flow (that is, the ratio of $\bar{w}$ to $\bar{u}$) behind each cylinder pair was roughly constant for elements of the same height across arrays. Several streamlines have been highlighted in the figure to illustrate this observation. For example, in the sawtooth array (top row), the short element at $x = 168D$, $y = -1D$ (second column) shows a strong vertical flow, which causes the streamline starting just above the cylinder ($5D$ in height) to reach the bottom of the array in a streamwise extent of only about $5D$: a flow angle of very nearly 45 deg. In the wedge array (second row), the short element at $x = 176D$, $y = -1D$ shows almost exactly the same trend. Similarly, for the tall elements in the sawtooth, wedge, and random arrays, the flow path indicates a vertical drop of only about $3.5D$ over a streamwise extent of $8D$: a flow angle of roughly 24 deg (streamlines showing this trend are highlighted in the $y = 0D$ plane, left column). The average height element in the sawtooth array shows an intermediate flow angle of around 32 deg. Surprisingly, the average height element in the uniform

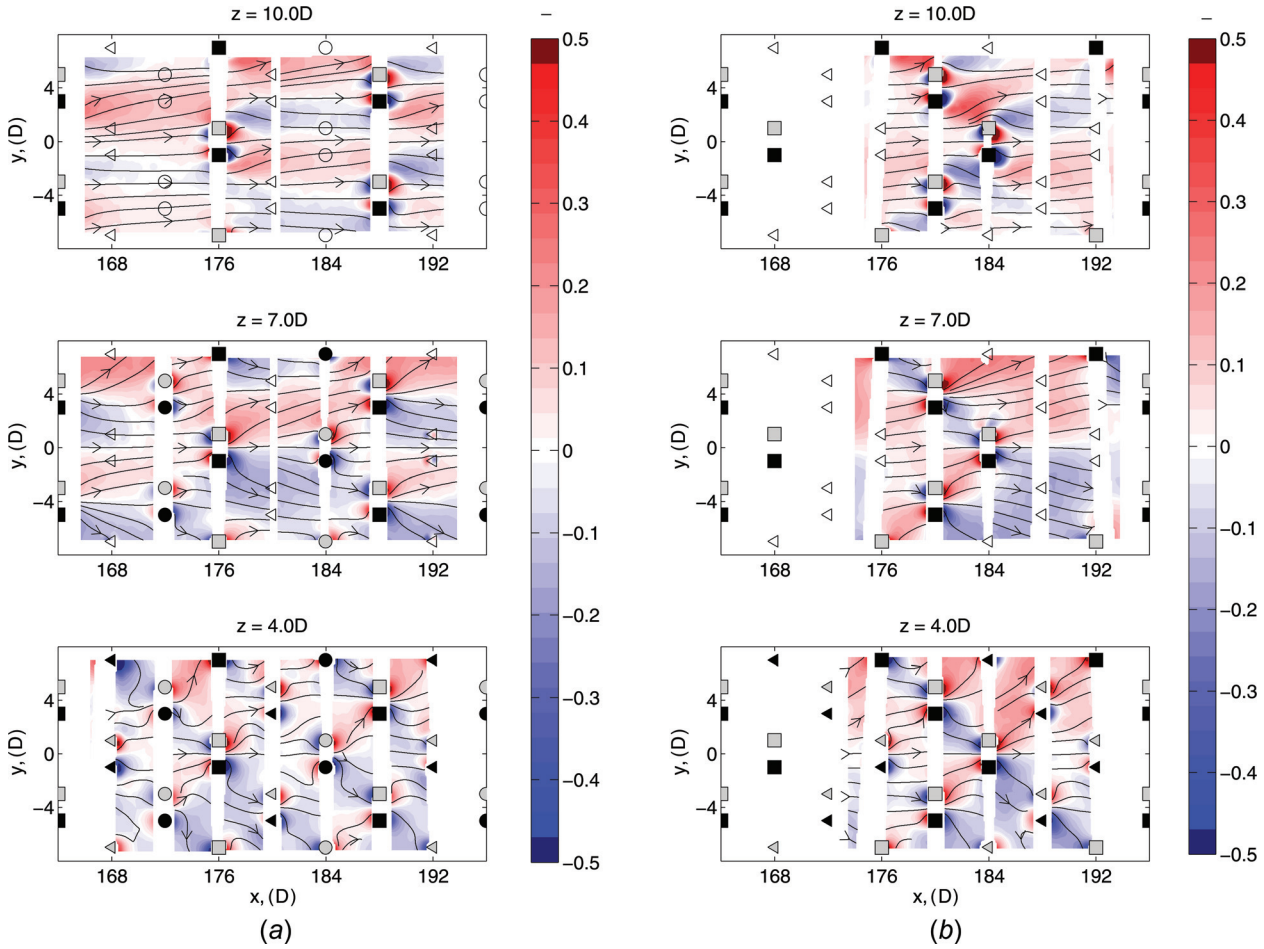

Fig. 5 Time-averaged transverse flows and streamlines in the three horizontal data planes for the (*a*) sawtooth and (*b*) wedge arrays, $\alpha = 2$. Here, as in Fig. 1, the symbol indicates the height of the element: ◁ indicates a short element, ○ indicates an average element, and □ indicates a tall element. The color of the symbol indicates the rotational direction as viewed from above (if the element intersects the given data sheet; if the element is below the height of the data sheet, the symbol is left white): black indicates clockwise rotation and gray indicates counterclockwise rotation. Note that the missing data along the rows of elements are due to shadowing of the laser sheet.

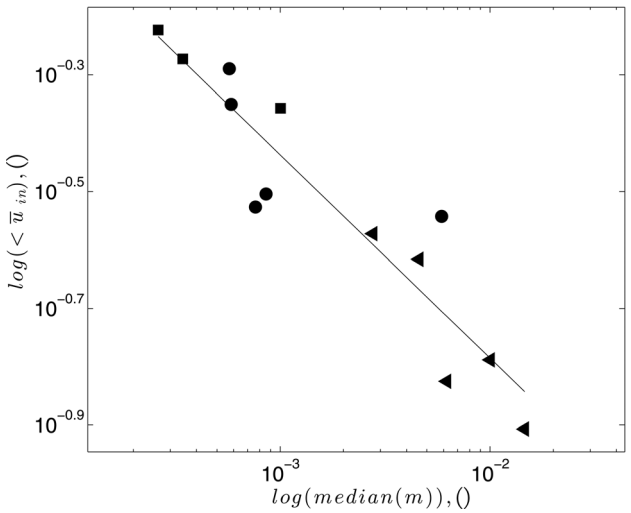

Fig. 6 Comparison between quantified meander of flow in the array and the performance of the array (for $\alpha = 2$ data). The symbol indicates the height of the data sheet: ◁ indicates that the data sheet was at or below $z = 5D$, ○ indicates that the data sheet was at or below $8D$, and □ indicates that the data sheet was at or below $11D$. Multiple symbols come from the different arrays. The solid line is the linear best fit: $R^2 = 0.86$.

array shows a flow angle much closer the tall elements in the heterogeneous-height arrays than to the average height element of the sawtooth array: the vertical drop is about $3D$ over an $8D$ streamwise extent, for a flow angle of roughly 21 deg.

These qualitative observations can be made much more quantitative: concentrating on the data taken at $y = 0D$, streamlines can be started at every point in a $0.5D \times 0.5D$ region centered on the trailing upper edge of each cylinder pair. These streamlines can be traced a finite distance (in this case, over roughly $8D$ in the streamwise direction, but stopping the trace within $1D$ of the bottom to avoid including bottom effects), and then, the median angle along each streamline and over all streamlines can be computed. The results of this analysis are presented in Table 1.

It is worthwhile to emphasize at this point that the flow angle is intended as an easily quantified surrogate for the strength of the vertical flow relative to the strength of the streamwise flow. In turn, the strength of the (time–space averaged) vertical flow has been shown to be well correlated with the performance of the array (see Sec. 3.1.1). Thus, by concentrating on the "angle" of the flows induced by the vertical structuring of the array, it is possible to represent the performance of the array, which is of primary interest.

Certainly, the spread in angles, both for a single element pair and between element pairs, was significant. However, in order to move forward with the analysis of vertical structure effects on vertical flow, it was taken as a rough approximation that the tallest

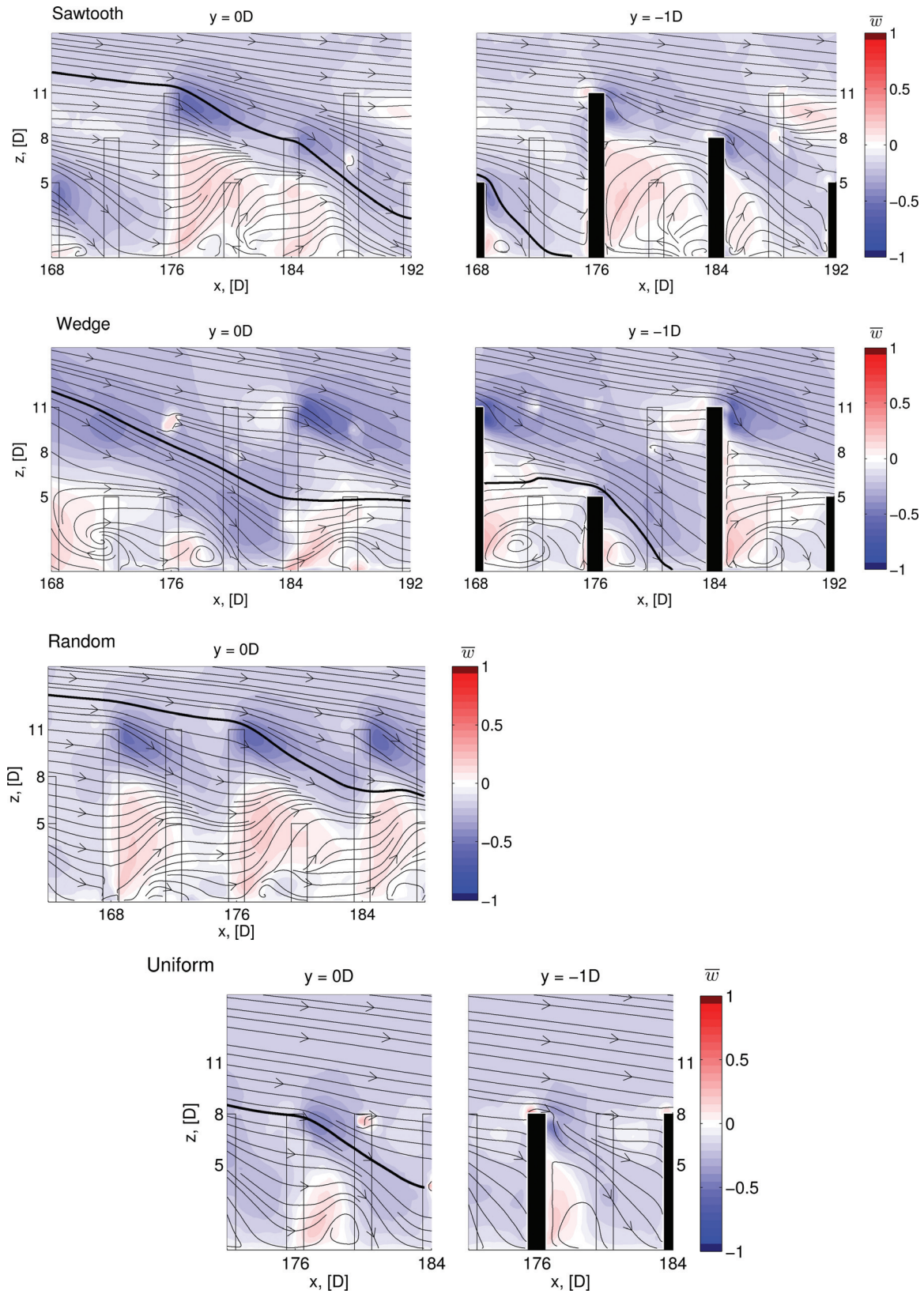

Fig. 7 Time-averaged vertical flow and streamlines for a selection of the vertical data sheets taken in each array, $\alpha = 2$. Solid black rectangles indicate that the sheet intersects with a clockwise rotating cylinder. Rectangle outlines indicate the locations of the rows which the laser sheet does not intersect, with the height of the element closest to the laser sheet being indicated. Please note that due to line of sight blocking by other elements along the rows, data were not able to be collected between elements in a row. Interpolation was used to fill these regions of missing data, and features "within" the outlined cylinders may be artifacts of the interpolation.

Table 1 Median angles of flow in near field behind each element pair

	Short (deg)	Average (deg)	Tall (deg)
Sawtooth	-45 ± 4	-36 ± 6	-26 ± 8
Wedge	-42 ± 10	—	-26 ± 4
			-29 ± 6
Random	—	—	-28 ± 8
			-29 ± 6
			-27 ± 7
Uniform	—	-27 ± 5	
		-28 ± 7	

Uncertainties reported are one standard deviation over the measurements.

element in a given array would induce a vertical flow at an angle of -27.5 deg, or equivalently $\bar{w}/\bar{u} = -0.52$. Again, making a rough approximation and taking $\bar{u}$ as constant over the range of interest, $\bar{w} = -0.52\bar{u}|_{z=H_{\max}}$. Furthermore, it was taken for the heterogeneous arrays that the average height elements and short height elements induced vertical flows at angles of -36 deg and -43.5 deg, respectively. Again, approximating $\bar{u}$ as constant over the region of interest, $\bar{w} = -0.73\bar{u}|_{z=8D}$ and $\bar{w} = -0.95\bar{u}|_{z=5D}$.

As an aside, the variation in flow angle may be associated with the ratio of the cylinder surface rotation speed to the local streamwise velocity near the top of the elements, that is, $\alpha_{\text{local}} = D\Omega/2u_{\text{local}}$, noting again that α is computed based on the freestream velocity, u_0. This hypothesis is motivated by noting that since u tends to decrease with height in the arrays, but the cylinder rotation remains constant for all cylinder heights, the α_{local} must increase even as the flow angles increase for the decreasing element heights. Formalizing this observation, in Fig. 8, the flow angles are compared against α_{local}, where u_{local} is computed over a $0.5D \times 0.5D$ region just in front of the upper edge of each cylinder pair, in each array configuration. (Note that the requirement of data upstream of the cylinder pair reduces the number of available data points.) From this comparison, it can be seen that flow angle magnitude does increase with increasing α_{local}, with a correlation coefficient for a linear relationship of $R^2 = 0.93$.

Continuing to develop the model, one further approximation can be made to relate $\bar{u}|_{z=5D,8D}$ to $\bar{u}|_{z=11D}$ for the heterogeneous-height arrays. Taking the average over all heterogeneous-height arrays, $(\bar{u}|_{z=5D})/(\bar{u}|_{z=11D}) = 0.3 \pm 0.1$ and $(\bar{u}|_{z=8D})/(\bar{u}|_{z=11D}) = 0.60 \pm 0.06$ (where the uncertainties are one standard deviation). Although the variation between arrays is significant, especially for the lower height in the arrays, in order to continue building a very simple model to relate vertical flow to vertical structure, scaling factors are defined in order to convert all estimates for vertical flow to units of $\bar{u}|_{z=H_{\max}}$. In the following, it is taken that $\xi_1 = (\bar{u}|_{z=5D})/(\bar{u}|_{z=11D}) = 0.3$ and $\xi_2 = (\bar{u}|_{z=5D})/(\bar{u}|_{z=11D}) = 0.6$.

Having now a (rough) estimate for the vertical flow induced by a pair of elements in an array, a prediction of the relative vertical flow can be made. The procedure is best described with reference to an example.

The first example taken will be the $y = -1D$ transect in the sawtooth array, as shown in Fig. 9, top panel. For the sawtooth, a repeating unit cell may be defined from $x = 168D$ to $192D$ and $y = -4D$ to $4D$. The solid and dashed vertical gray lines (blue online) indicate the streamwise extent of the cell. First, the appropriately angled "streamlines" are drawn in: the solid gray lines (red online) starting at the top of each intersected cylinder and extending either to the bottom or to an intersection with another element. Over that determined streamwise extent, the appropriate vertical flow value (scaled to $\bar{u}|_{z=H_{\max}}$) is assigned. In this case, the short element contributes $-0.95\xi_1\bar{u}|_{z=H_{\max}}$ over $5.26D$, the tall element contributes $-0.52\bar{u}|_{z=H_{\max}}$ over $8D$, and the medium element contributes $-0.73\xi_2\bar{u}|_{z=H_{\max}}$ over $8D$. The average flow over the streamwise extent of the cell ($24D$) is therefore (using the defined scalings ξ_1 and ξ_2) $[(-095(03)(526) + -073(06)(8) + -052(8))/24] = -0.38\bar{u}|_{z=H_{\max}}$. This process is then repeated for each transverse position which intersects a cylinder in the selected unit cell of the array. For the cell selected in the sawtooth array, this is $y = [-3D, -1D, 1D, 3D]$. For the sawtooth array, however, all transects are effectively identical, and therefore, the average vertical flow prediction for the array is $-0.38\bar{u}|_{z=H_{\max}}$.

The second example taken will be the $y = -3D$ transect in the random array, as shown in Fig. 9, bottom panel. In this case, there is no repeating unit cell, so the cell under consideration is defined to be from $x = 168D$ to $192D$ and $y = -4D$ to $4D$. The solid and dashed vertical gray lines (blue online) indicate the streamwise extent of the cell. In this case, the intersected elements are not at

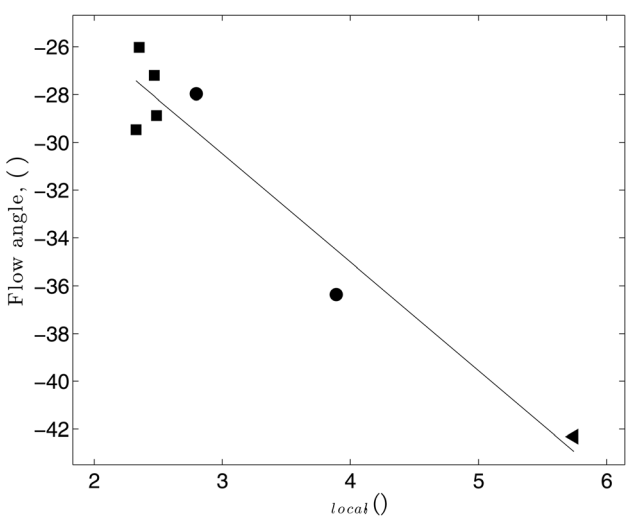

Fig. 8 Comparison of the flow angle behind each cylinder pair with the local tip-speed ratio ($\alpha = 2$ data). The symbol indicates the height of the element pair: ◁ indicates a short element pair, ○ indicates an average element pair, and □ indicates a tall element pair. The solid line indicates the linear best fit: $R^2 = 0.93$.

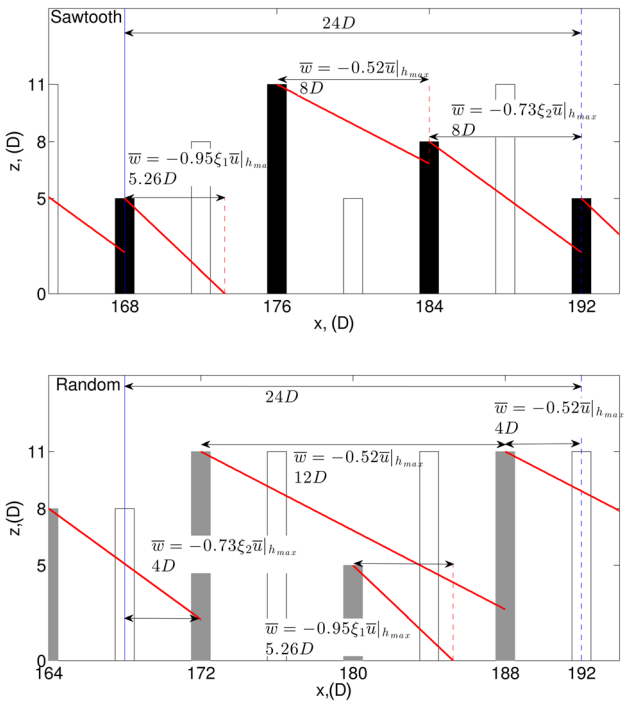

Fig. 9 Illustrations of vertical flow prediction based on vertical structuring of array: top panel—sawtooth array, $y = -1D$ and bottom panel—wedge array, $y = -3D$

the edges of the defined cell, so care must be taken to correctly take into consideration the induced vertical flow from elements outside of the cell, as shown here for the average height element at $x = 164D$. Following the same procedure of tracing an appropriately angled streamline from the top of each intersected element to either the bottom or intersection with another element in this case yields a short element contribution of $-0.95\xi_1\bar{u}|_{z=H_{\max}}$ over $5.26D$, a medium element contribution of $-0.73\xi_2\bar{u}|_{z=H_{\max}}$ over $4D$, and two tall element contributions totaling $-0.52\bar{u}|_{z=H_{\max}}$ over $16D$. The average vertical flow along this transect is therefore $[(-0.95(03)(5.26) + -0.73(0.6)(4) + -0.52(16))/24] = -0.48\bar{u}|_{z=H_{\max}}$. The required transects in this case are $y = [-3D, -1D, 1D, 3D]$. Repeating the procedure for the other three transects yields $-0.52\bar{u}|_{z=H_{\max}}$ at $y = -1D$, $1D$ and $-0.19\bar{u}|_{z=H_{\max}}$ at $y = 3D$. The average for the array is therefore $-0.33\bar{u}|_{z=H_{\max}}$.

Using this procedure for the wedge array and the uniform array yields $-0.61\bar{u}|_{z=H_{\max}}$ and $-0.52\bar{u}|_{z=H_{\max}}$, respectively.

Assuming that $\bar{u}|_{z=H_{\max}}$ is constant across arrays, these values can be compared to each other, and taking $\bar{u}|_{z=H_{\max}} = 0.7u_0$, these values can be compared to the time–space averaged vertical flow evaluated at the maximum height of each array ($\langle\bar{w}\rangle|_{z=H_{\max}}$, in units of u_0). The comparison (as shown in Fig. 10) is linear across all array configurations to a correlation coefficient of 0.99; however, the absolute values are significantly different. Thus, while the method proposed here is capable of predicting the relative vertical flows between different array vertical structures, it is not capable of quantitatively predicting the vertical flow magnitude. Nevertheless, a particular strength of the model is the conversion from a characteristic of an array not necessarily intuitive (the incoming streamwise velocity to the elements) to a characteristic which is easily visualized and "optimized" (the angle of the flow behind elements.) For example, in the sawtooth array, the lowest performing array, the modeled streamlines from one element intersect an element in the very next row, allowing very little vertical transport of streamwise momentum to develop. Conversely, in the wedge array, the highest performing array, the modeled streamlines from a tall element intersect another element only after traveling two rows in the streamwise direction, allowing much more vertical transport of streamwise momentum.

Before leaving this section, it should be noted that the empirical nature of the proposed method makes it specific to the examined spatial configuration of the elements. Other configurations, such as different element densities, would be expected to change these results, although our sense is that the qualitative trends will remain largely the same, allowing simply a recalibration of the same underlying model.

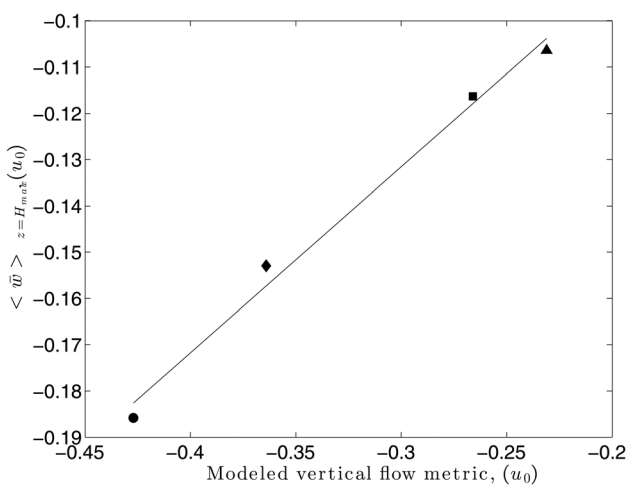

Fig. 10 Comparison of model predicted vertical flow and measured vertical flow at the maximum height of the array ($\alpha = 2$ data). The symbol indicates the array: □ indicates the sawtooth array, ○ indicates the wedge array, △ indicates the random array, and ◇ indicates the uniform height array. The solid line indicates the linear best fit: $R^2 = 0.99$.

3.3 Turbulence Characteristics. Focusing on the vertical variations in turbulence, the spatially averaged profiles of the quadrant-based decomposition of Reynolds shear stress behavior may be examined. In brief (for more details see, e.g., Refs. [10,28]), the four quadrants are defined and denoted as Q1: $u' > 0, w' > 0$, Q2: $u' < 0, w' > 0$, Q3: $u' < 0, w' < 0$, and Q4: $u' > 0, w' < 0$. The pertinent quantities are given by

$$H = \frac{|u'w'_{\text{threshold}}|}{|\overline{u'w'}|} \tag{2}$$

$$I_{i,H,t}(u', w', t) = \begin{cases} 1 & (u'w') \in i, |u'w'| \geq H|\overline{u'w'}| \\ 0 & \text{otherwise} \end{cases} \tag{3}$$

$$S = \frac{1}{T}\sum_t |u'(x,z,t)w'(x,z,t)|dt \tag{4}$$

$$S_{i,H} = \frac{1}{T}\sum_t |u'(x,z,t)w'(x,z,t)|I_{i,H,t}(x,z,t)dt \tag{5}$$

$$S^f_{i,H} = \frac{S_{i,H}}{S} \tag{6}$$

$$D^f_{i,H} = \frac{1}{T}\sum_t I_{i,H,t}dt \tag{7}$$

The stress fraction, denoted $S^f_{i,H}$, represents the fraction of the total stress at a given point in space which is contributed by event type i, above a certain threshold stress level H, using the conditional sampling function I. The duration fraction, denoted $D^f_{i,H}$, represents the fraction of the total measurement time for which a point in space is experiencing an event of type i, above a certain threshold stress level H.

Within the present context, it is again the transfer of momentum into and out of the array which is of primary interest to understand. The discussion is therefore cast in terms of comparing Q2 and Q4 events against Q1 and Q3 events. The Q2 and Q4 events contribute positively to a higher momentum within the array either by "ejecting" a locally lower momentum upward, out of the array or by "sweeping" a locally higher momentum downward into the array, respectively. The Q1 and Q3 events contribute negatively to a higher momentum within the array either by bringing locally higher momentum up out of the array or by bringing locally lower momentum down into the array, respectively. The focus is, therefore, not placed on comparing the different arrays against each other, but on extracting the effects of the array's vertical structure on the relative balance of Q2/Q4 versus Q1/Q3 events within each array.

In the present analysis, events of all stress magnitudes will be considered by setting $H = 0$. Figure 11 presents the spatially averaged profiles of the stress fractions (11(*a*)) and duration fractions (11(*b*)) within the arrays.

The general pattern followed by the four arrays is Q4 stress fraction domination and Q2 duration fraction domination below around $z = 0.75H_{\max}$ and Q2 stress fraction and Q4 duration fraction domination above that point. The one notable deviation from this trend is the wedge array, where the Q2 and Q4 stress and duration fractions are almost balanced between $z = 0.5$–$0.75H_{\max}$). For all arrays, the Q1 and Q3 stress and duration fractions are significantly lower throughout the arrays and tend to follow each other closely, indicating little symmetry-breaking mechanism within the arrays in this regard. These patterns are in agreement with previously reported results for stationary (roughly) homogeneous-height canopies [28].

The importance of examining the quadrant-based decomposition of the Reynolds stresses for these arrays, therefore, is the

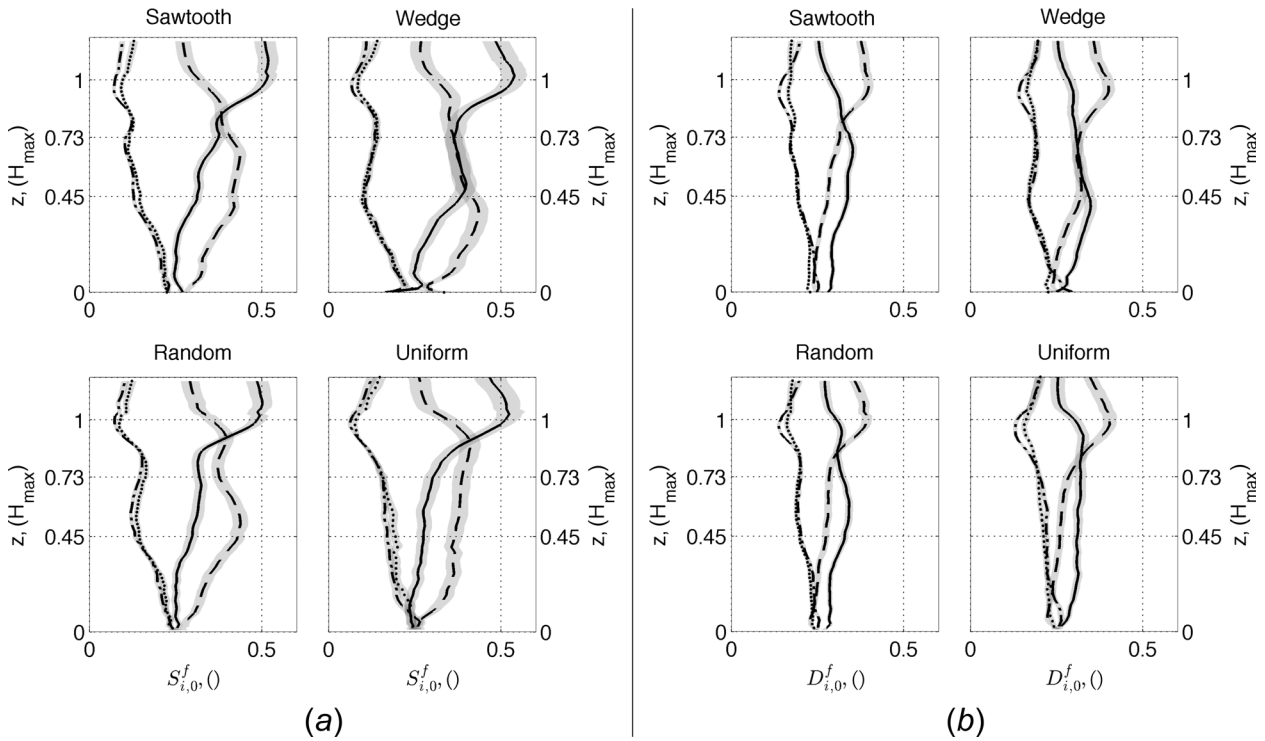

Fig. 11 Time–space averaged stress fraction (*a*) and duration fraction (*b*) of $u'w'$ events in quadrant 1 (–·), quadrant 2 (–), quadrant 3 (··), and quadrant 4 (– –). Hole size = 0 for each of the four arrays.

finer-scale detail within these general trends. It may be observed that at each of the element heights present in a given array (e.g., short, average, and tall in the sawtooth array, but only short and tall in the wedge array), there are small, vertically localized increases in the Q2/Q4 stress and duration fractions and corresponding decreases in the Q1/Q3 stress and duration fractions. The only notable deviation is that in the random array, the shifts are not apparent at the average element height; this is likely due to few average height elements in the specific measurements taken.

Physically, this may be interpreted as the vertical structuring of the arrays acting to organize the turbulence in a manner beneficial for increased momentum within the array: at the heights of the elements present in the arrays, the momentum-lowering Q1/Q3 events are replaced by stronger Q4 (sweep) events and more frequent or more temporally persistent Q2 (ejection) events, both of which act to increase the momentum in the array. This beneficial organizing effect was noted previously in the examination of the turbulence-driven vertical flux of streamwise momentum which showed peaks at the heights of the elements present in each of the arrays (Sec. 3.1.1, Fig. 4). It is noted that this organization effect is seen in all arrays, including those with relatively lower performance, although the effect is perhaps strongest in the best-performing wedge array.

4 Conclusions and Future Work

It has been shown that the vertical structuring of an array of rotating cylinders, created by using elements of varying heights, has the potential to alter both mean and turbulent flow characteristics within the array. Reynolds stress events have been shown to become more organized at the heights of the elements in the array, favoring stronger and more frequent or temporally persistent sweep and ejection events, both of which positively impact the momentum resource within the array. The net effect of this organization is clear in the examination of the vertical flux of streamwise momentum in the array, which shows peaks in the momentum flux being brought down into the array from above at each of the element heights present in a given array.

The primary contribution to the vertical flux of streamwise momentum, however, is the mean-driven flux, which is itself directly dependent on the vertical structuring of the array. A rough model has been proposed, which allows the influence of the vertical structuring on the mean vertical flow into the array to be predicted, relative to other arrays with same rotation rate and spatial/rotational geometry. The model is based on a simplified conceptual understanding of the vertical flows: the downward mean vertical flows are initiated behind each pair of elements and continue to penetrate into the array until aborted by the presence of another pair of elements. Thus, by carefully choosing the streamwise sequence of element heights, the interruptions of this vertical inflow may be minimized, corresponding to a greater injection of streamwise momentum from above the array.

Of particular note in this model is the suggestion that the angle of the flow behind each pair of cylinders is related to the ratio of the cylinder surface rotational speed and the local streamwise velocity. If this proposal is correct, it could be possible to tune the rotation rates of the different height elements in order to either maximize the vertical flows into the array or minimize the spatial variations in vertical flow such that the shear instabilities within the array might be reduced.

Within the array, it has also been shown that large-scale horizontal flow patterns can be developed between elements, which can channel the introduced streamwise momentum into the elements rather than diverting or dissipating the momentum, resulting in an improved overall performance. Most importantly, it has been shown that the patterns have vertical persistence: the flow patterns established at the higher heights in the array (by only the taller elements) can influence the transverse flow patterns at the lower heights in the array (intersecting more elements). Thus, the beneficial channeling or the adverse diversion of the flow between pairs of elements in an array can be influenced by the vertical structure of the array.

Cumulatively, the improvement in streamwise momentum resource between arrays of different vertical structures could show up to a 56% improvement from the lowest to highest resource arrays. Such significant improvement in the performance

of the arrays may be taken as motivation to examine in more detail the potential of heterogeneous-height VAWT arrays for improved array power output. Finally, given the importance of flow channeling within the horizontal plane, it would be of interest to examine the potential of stationary elements being added to a rotating element array as flow "guides."

Acknowledgment

This work was supported by funding to A.E.C. from an NSF Graduate Research Fellowship and a Stanford Graduate Fellowship, by funding to J.O.D. from ONR N000141211047 and the Gordon and Betty Moore Foundation through Grant GBMF2645, and by funding from the Bob and Norma Street Environmental Fluid Mechanics Laboratory at Stanford University.

References

[1] Chan, A. S., Dewey, P. A., Jameson, A., Liang, C., and Smits, A. J., 2011, "Vortex Suppression and Drag Reduction in the Wake of Counter-Rotating Cylinders," J. Fluid Mech., **679**, pp. 343–382.
[2] Guo, X., Lin, J., Tu, C., and Wang, H., 2009, "Flow Past Two Rotating Circular Cylinders in a Side-by-Side Arrangement," J. Hydrodyn., **21**(2), pp. 143–151.
[3] Kumar, S., Gonzalez, B., and Probst, O., 2011, "Flow Past Two Rotating Cylinders," Phys. Fluids, **23**(1), p. 014102.
[4] Ueda, Y., Kida, T., and Iguchi, M., 2013, "Steady Approach of Unsteady Low-Reynolds-Number Flow Past Two Rotating Circular Cylinders," J. Fluid Mech., **736**, pp. 414–443.
[5] Yoon, H. S., Kim, J. H., Chun, H. H., and Choi, H. J., 2007, "Laminar Flow Past Two Rotating Circular Cylinders in a Side-by-Side Arrangement," Phys. Fluids, **19**(12), p. 128103.
[6] Yoon, H. S., Chun, H. H., Kim, J. H., and Park, I. L. R., 2009, "Flow Characteristics of Two Rotating Side-by-Side Circular Cylinder," Comput. Fluids, **38**(2), pp. 466–474.
[7] Whittlesey, R. W., Liska, S., and Dabiri, J. O., 2010, "Fish Schools as a Basis for Vertical Axis Wind Turbine Farm Design," Bioinspiration Biomimetics, **5**(3), p. 035005.
[8] Dabiri, J. O., 2011, "Potential Order-of-Magnitude Enhancement of Wind Farm Power Density Via Counter-Rotating Vertical-Axis Wind Turbine Arrays," J. Renewable Sustainable Energy, **3**(4), p. 043104.
[9] Kinzel, M., Mulligan, Q., and Dabiri, J. O., 2012, "Energy Exchange in an Array of Vertical Axis Wind Turbines," J. Turbul., **13**(38), pp. 1–13.
[10] Craig, A., Dabiri, J., and Koseff, J., 2016, "A Kinematic Description of the Key Flow Characteristics in an Array of Finite-Height Rotating Cylinders," ASME J. Fluids Eng., **138**(7), p. 070906.
[11] Weitzman, J. S., Zeller, R. B., Thomas, F. I. M., and Koseff, J. R., 2015, "The Attenuation of Current- and Wave-Driven Flow Within Submerged Multispecific Vegetative Canopies," Limnol. Oceanogr., **60**(6), pp. 1855–1874.
[12] Cheng, H., and Castro, I. P., 2002, "Near Wall Flow Over Urban-Like Roughness," Boundary-Layer Meteorolo., **104**(2), pp. 229–259.
[13] Kanda, M., 2006, "Large-Eddy Simulation on the Effects of Surface Geometry of Building Arrays on Turbulent Organized Structures," Boundary-Layer Meteorol., **118**(1), pp. 151–168.
[14] Xie, Z. T., Coceal, O., and Castro, I. P., 2008, "Large-Eddy Simulation of Flows Over Random Urban-Like Obstacles," Boundary-Layer Meteorol., **129**(1), pp. 1–23.
[15] Jiang, D., Jiang, W., Liu, H., and Sun, J., 2008, "Systematic Influence of Different Building Spacing, Height, and Layout on Mean Wind and Turbulent Characteristics Within and Over Urban Building Arrays," Wind Struct., **11**(4), pp. 275–289.
[16] Hagishima, A., Tanimoto, J., Nagayama, K., and Meno, S., 2009, "Aerodynamic Parameters of Regular Arrays of Rectangular Blocks With Various Geometries," Boundary-Layer Meteorol., **132**(2), pp. 315–337.
[17] Millward-Hopkins, J. T., Tomlin, A. S., Ma, L., Ingham, D., and Pourkashanian, M., 2011, "Estimating Aerodynamic Parameters of Urban-Like Surfaces With Heterogeneous Building Heights," Boundary-Layer Meteorol., **141**(3), pp. 443–465.
[18] Ferreira, C. S., Madsen, H. A., Barone, M., Roscher, B., Deglaire, P., and Arduin, I., 2014, "Comparison of Aerodynamic Models for Vertical Axis Wind Turbines," J. Phys.: Conf. Ser., **524**, p. 012125.
[19] Shamsoddin, S., and Porte-Agel, F., 2014, "Large Eddy Simulation of Vertical Axis Wind Turbine Wakes," Energies, **7**(2), pp. 890–912.
[20] Archer, C., Xie, S., Ghaisas, N., and Meneveau, C., 2015, "Benefits of Vertically-Staggered Wind Turbines From Theoretical Analysis and Large-Eddy Simulations," North American Wind Energy Academy Symposium, Blacksburg, VA, June 9–11, pp. 3–6.
[21] Nikora, V., Ballio, F., Coleman, S., and Pokrajac, D., 2013, "Spatially Averaged Flows Over Mobile Beds: Definitions, Averaging Theorems, and Conservation Equations," J. Hydraul. Eng., **139**(8), pp. 803–811.
[22] Craig, A., and Dabiri, J. O., 2015, "V-Shaped Arrangements of Turbines," U.S. Patent No. 9,175,669 B2.
[23] Efron, B., and Tibshirani, R. J., 1993, *An Introduction to the Bootstrap* (Monographs on Statistics and Applied Probability, Vol. 57), Chapman & Hall, New York.
[24] Theunissan, R., Sante, A. D., Riethmuller, M. L., and den Braembussche, R. A. V., 2008, "Confidence Estimation Using Dependent Circular Block Bootstrapping: Application to the Statistical Analysis of PIV Measurements," Exp. Fluids, **44**(4), pp. 591–596.
[25] Patton, A., 2014, "MATLAB Codes."
[26] Cal, R. B., Lebrón, J., Castillo, L., Kang, H. S., and Meneveau, C., 2010, "Experimental Study of the Horizontally Averaged Flow Structure in a Model Wind-Turbine Array Boundary Layer," J. Renewable Sustainable Energy, **2**(1), p. 013106.
[27] Calaf, M., Meneveau, C., and Meyers, J., 2010, "Large Eddy Simulation Study of Fully Developed Wind-Turbine Array Boundary Layers," Phys. Fluids, **22**(1), p. 015110.
[28] Yue, W., Meneveau, C., Parlange, M., Whu, W., van Hout, R., and Katz, J., 2007, "A Comparative Quadrant Analysis of Turbulence in a Plant Canopy," Water Resources Research, **43**(5), (epub May 17, 2007).